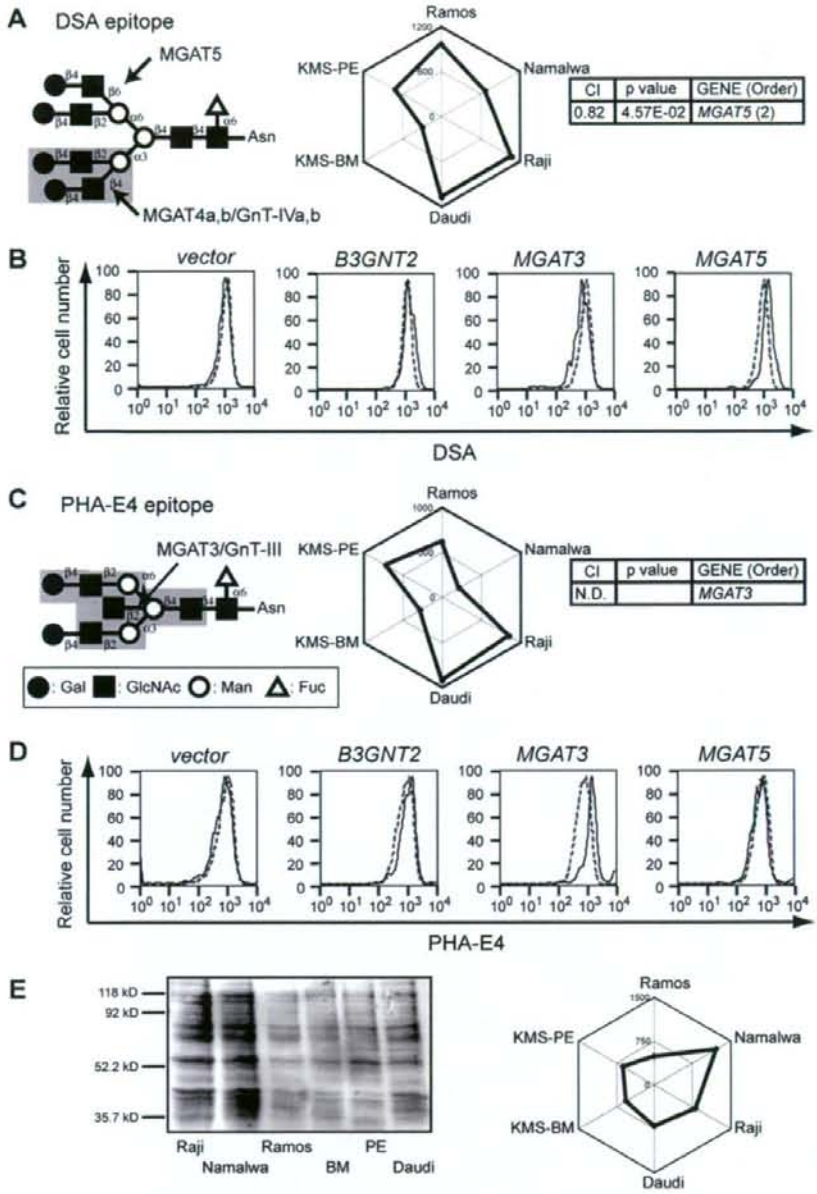

Figure 4. CIRES analyses of staining profiles obtained using lectins that recognize internal glycan structures and have unknown epitope-expression-regulating enzymes. Presentation is the same as in Fig. 2 except that the plant lectins used were **(A, B)** DSA and **(C–E)** PHA-E4. N.D. in the gene order list indicates that no significant correlation was detected. **(B, D)** Flow cytometric staining patterns for EGFP-positive Namalwa cells are shown in bold lines, and those for EGFP-negative (control) cells are shown in gray dashed lines. The overexpression of *MGAT5* resulted in a subtle (60%) increase in DSA staining. The overexpression of *MGAT3* resulted in a 2-fold increase in PHA-E4 staining. **(E)** PHA-E4 lectin blotting was performed using the membrane fraction of the same set of cell lines. A plot of the quantified signals reveals differences in the PHA-E4 staining profile among the six cell lines (C, E), as discussed in the text.
doi:10.1371/journal.pone.0001232.g004

staining, probably reflecting the GlcNAc-binding aspect of WGA. In a case such as this one, the correlation of the genes identified by CIRES may appear to be additive, but a lack of exclusivity tends to reduce the correlation index for each gene.

***Canavalia ensiformis* lectin (Con-A)** The modification of N-glycans occurs following the transfer of lipid-linked Glc_3-Man_9-$GlcNAc_2$ to nascent N-glycosylated protein by oligosaccharyl-transferase in the ER [39]. Con-A recognizes mannose (Man)-

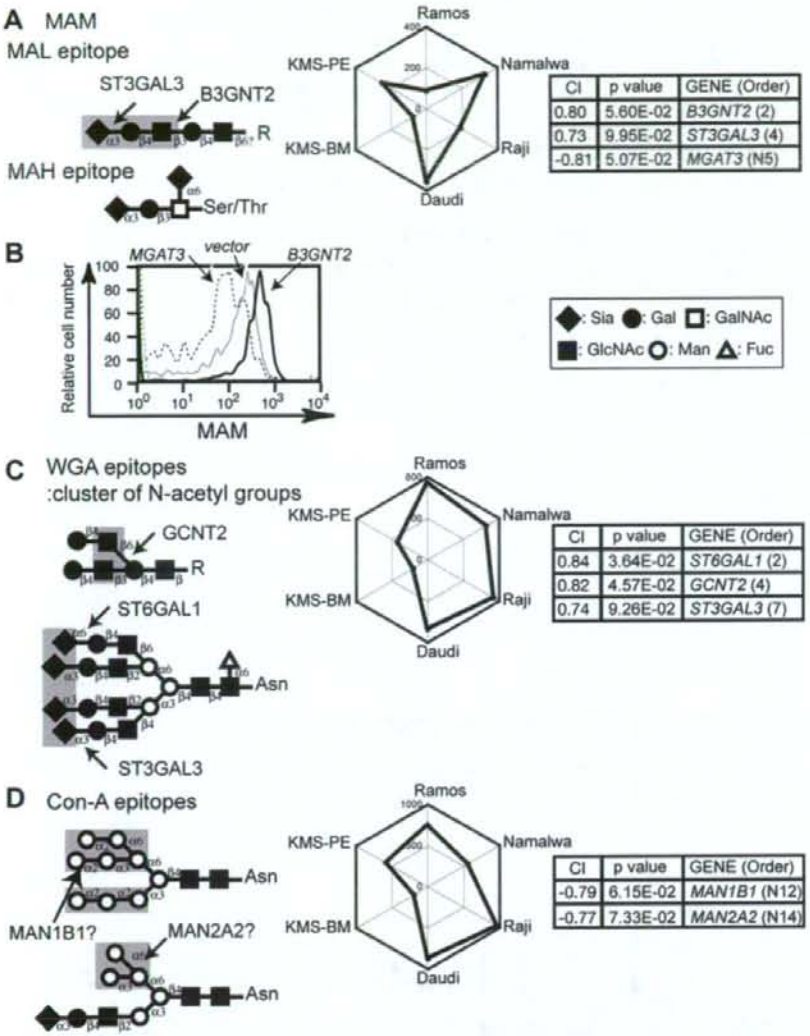

Figure 5. CIRES analyses of staining profiles obtained using lectins that recognize multiple glycan structures and have unknown epitope expression-regulating enzymes. Presentation is the same as in Fig. 2 except that the plant lectins used were (**A–B**) MAM, (**C**) WGA, and (**D**) Con-A. The epitopes of the two different lectins of MAM, MAL and MAH, are illustrated separately. WGA essentially recognizes a cluster of N-acetyl groups, as indicated, and thus required Neu5Ac as a Sia species. Con-A recognizes mannose-containing glycans with varying affinities. High-mannose-type glycans (upper diagram in (**D**)) bind best to this lectin. (**B**) Namalwa cells were infected with retroviruses encoding various GlcNAc transferases. The MAM staining patterns of the EGFP-positive populations of each infectant are shown. *MGAT5* overexpression did not shift the staining pattern in comparison with the vector control (data not shown).
doi:10.1371/journal.pone.0001232.g005

containing N-glycans to various degrees; it binds preferentially to high-mannose N-glycans, followed by hybrid-type N-glycans, and has the least affinity for complex-type N-glycans. In theory, oligosaccharyltransferase activity is required for the expression of the Con-A epitope, whereas mannosidase expression is inhibitory. Con-A staining profiles revealed a subtle but significant negative correlation with the expression of the mannosidase genes *MAN1B1* and *MAN2A2* (Figure 5D). Thus, the mannosidases encoded by these genes may control the expression of high-mannose N-glycans on the cell surface. Alternatively, other factors such as the expression of the protein moiety of the glycoconjugate could determine the expression of the Con-A epitope, given that the number of proteins reported to carry high-mannose glycans is limited.

***Agaricus bisporus* agglutinin (ABA)** ABA recognizes Gal-exposed core-1 structures that are similar to the PNA epitope, but in contrast to PNA, ABA can recognize sialylated structures [40]. In B cells, ABA staining was similar to PNA staining and was negatively correlated with *ST3GAL1* expression (Figure 6A). Consistent with this negative correlation, ABA binding was increased in Daudi cells treated with sialidase (Figure 6B), similar to the enhanced binding of PNA observed upon sialidase treatment. This effect occurred with both a broad-range sialidase

(*Arthrobacter ureafaciens* sialidase, AUS) and the $\alpha_{2,3}$-linked Sia-specific *Salmonella typhimurium* sialidase (Figure 6B), indicating that sialylation, which probably occurs on the core-1 Gal residue, somehow inhibits recognition by ABA.

B3GNT5 expression positively correlated with ABA staining. In fact, a recent study has shown that ABA has dual specificity for glycan chains, recognizing both Gal-exposed O-glycans and GlcNAc-exposed N-glycans [41]. Whether the GlcNAc residue biosynthesized by the GlcNAc transferase is uncapped on the cell surface is unknown, but some ABA binding to GlcNAc may contribute to the increased correlation index of *B3GNT5* as compared with that for PNA, which showed an otherwise similar staining profile for the correlated genes.

Overall findings

As confirmed by staining with various plant lectins, CIRES successfully identified enzyme genes known to be involved in the biosynthesis of lectin-binding determinants. When an unbiased set of 15 lectins was analyzed for binding to six B-cell lines, 12 of the lectins showed significant staining. Correlation assessment of these staining profiles identified the enzyme genes that are apparently responsible for the expression of the specific epitopes for nine lectins. In general, lectins that recognize terminal structures of the glycan chain tended to yield the most reliable correlation with the responsible genes.

Interestingly, CIRES also found negative correlations for some epitopes, which is consistent with the fact that CIRES results are highly dependent on the regulatory mechanisms of glycan epitope expression, some of which are negative (*i.e.*, capping of an epitope by further glycosylation). Finding negative relationships is difficult in normal biological experimental setups but may have been possible using CIRES because of the unbiased correlation coefficient calculation resulting from the large set of cross-sample comparisons.

DISCUSSION

CIRES correlation analysis of glycan-related gene expression and binding of anti-glycan probes such as lectins

The functional glycans expressed on a cell surface can encode biological information. Although glycan-glycan interactions are important in determining the biological consequences of some glycosylations [42], glycan-binding proteins are the major target of functional glycans. Thus, the binding of glycan-specific proteins can be highly informative in decoding the glycomic information of an organism [43], making glycan-binding proteins a rational choice for the analysis of glycan expression. Although the identification of the proteins that bind best to each glycan is no doubt important given the role of glycan-binding proteins in glycan recognition in an organism [44,45], here we opted to

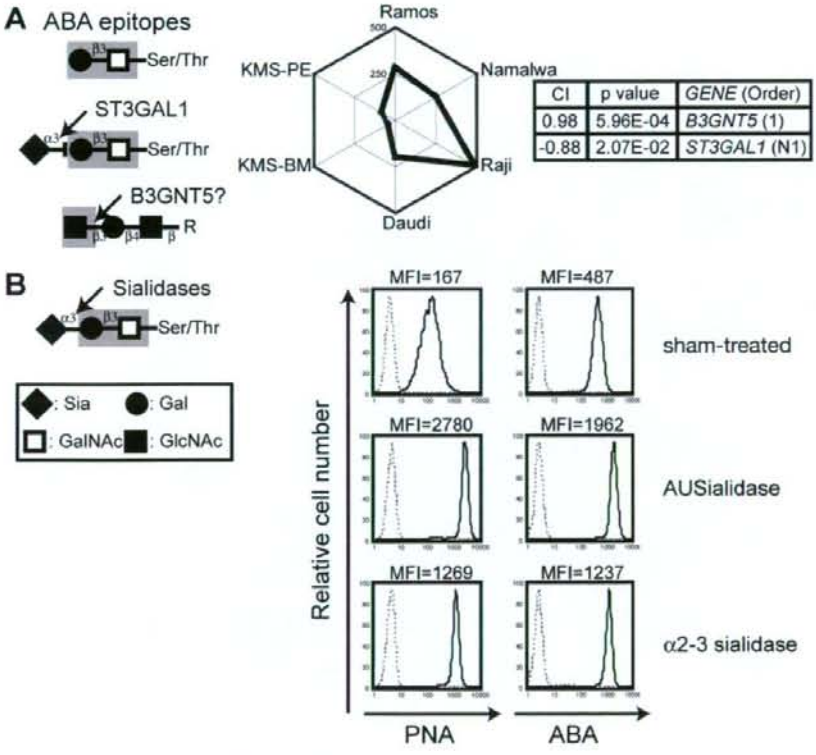

Figure 6. CIRES analyses of staining profiles obtained using the lectin ABA. (A) Presentation is the same as in Fig. 2 except that ABA was used. **(B)** Effect of sialidase treatment on the binding of ABA and PNA in B cells. (See text for the specificity of the sialidase and Fig. 2D for the PNA epitope.) Mean fluorescence intensity (MFI) values for the staining with each lectin (bold lines) are shown at the top. Dashed lines indicate the results from the non-staining control.

doi:10.1371/journal.pone.0001232.g006

identify the genes involved in the biosynthesis of specific glycans because, as the glycan-biosynthesis enzymes are responsible for producing the glycan ligands, this information will help elucidate the regulation of biological events mediated by glycan-binding proteins.

Systematic methodological merit of CIRES

The experimental setup for CIRES is relatively simple. Briefly, we first made a cross-sample comparison of glycan-related gene expression profiles using cDNA microarrays. This technique yielded the relative expression level for each gene as compared with a universal reference RNA, producing an expression profile for each gene. We then used anti-glycan lectin probes to obtain binding profiles in the same cell lines and compared the two types of profiles. We used the same cross-sample profiles of glycan-related gene expression for the correlation analyses of all the lectins examined in this study.

The cells that we used for gene expression profiling are available either commercially or from a non-profit cell resource center (Japanese Collection of Research Bioresources; JCRB). All cells were cultured under commonly used conditions and were used in logarithmic growth phase. Under these conditions, the glycan expression phenotype obtained by lectin staining tended to be uniform within a cell line and unique for each cell line. Thus, the data obtained by lectin staining with excess probe were suitable for determining the mean fluorescence intensity (MFI) of lectin staining.

This method compared the relative glycan expression profiles of cell lines whose cellular size and character might not be uniform; therefore, we normalized the staining signal by using the ratio of the stained sample MFI to the control MFI. This eliminates the absolute glycan expression signals and normalizes the relative expression results to the staining and data acquisition conditions.

The statistical analysis is the core of the CIRES method. Since glycosylation follows a defined pathway, we could have set up an algorithm suitable for the correlation analyses. However, we chose to use the well-established Pearson's correlation coefficient for the analyses. Regardless of the calculation method, correlations were detected even when the profiles did not completely match. Based on these calculations, a list of genes can be ordered according to the strength of their correlation. This list might be useful in designing further experiments to confirm biological functions.

In glycan biosynthesis, not all relationships are positive in nature, and some lectins used in this study yielded negative correlations. Thus, it is possible to detect dominant inhibitors of specific glycan biosynthesis steps using CIRES. Moreover, in theory, CIRES is not limited to glycan biosynthesis but could be used in any system for which numeric phenotypic expression results (such as glycan expression) can be obtained for a set of cultured cells. The correlation of non-glycosylation phenotypes with gene expression in the same system should be possible.

Systematic methodology for using microarray data in CIRES

One limitation of the standard microarray technique is that it can only detect the relative cDNA expression levels of two samples. This was actually useful when we took the ratio of the signal for each gene relative to that for reference RNA, thus circumventing the microarray problems associated with spot-to-spot variation and hybridization variation for different nucleotide sequences. Almost all of the spots hybridized with universal reference RNA (data not shown). Normal, uniform cell culture conditions were used in this experiment to maximize reproducibility.

In order to calculate the gene expression ratios in a cross-sample manner, we wanted to avoid negative signals in the microarray scans. To do this, we directly used the raw data, instead of applying a cut-off value to the microarray signal by deducting the local background signal from the raw spot signals. We consider this to be a valid option, because we confirmed that the scanner readout after hybridization was reproducible, even for spots yielding weaker signals, and that both options yielded a similar order of relative strength (data not shown).

Normalization was also important because the array results were compared in a cross-sample manner. Sum-based normalization was applied to obtain better correlation coefficients for proven lectins (data not shown). The validity of the calculations was dependent on the use of a consistent standard, making a universal reference essential for the cross-sample comparison. In general, the microarray results tended to be more consistent for stronger hybridization signals than for weaker signals.

Expected and unexpected findings with CIRES

For an epitope whose expression is regulated by a single gene product in its biosynthetic pathway and for which the supply of substrate for that biosynthetic reaction is abundant, CIRES will identify the gene involved in the biosynthesis of the epitope. The finding that the RCA120staining profile did not correlate with a specific glycosyltransferase was therefore not surprising, because it binds LacNAc. Generally, we obtained better correlation coefficients for epitopes created by terminal modifications of LacNAc. CIRES was also useful in identifying major genes responsible for epitope capping, which is negatively correlated with glycan expression, as in the case of PNA.

Our CIRES results tended to show correlations with the GlcNAc transferases. This may result from the use of flow cytometry to detect lectin binding, and thus glycan expression, because lectin staining preferentially detects glycans that extend beyond the glycocalyx. Moreover, the level of epitope expression may not linearly correlate with the lectin signal, because lectins tend to form multimers. As poly-LacNAcs are the usual core units for the presentation of some functional glycan epitopes, GlcNAc transferases found to correlate could also be important for the epitope presentation suitable for lectin-based recognition.

Thus far, we have not identified any enzymes other than glycosyltransferases that strongly correlate with epitope expression levels. However, a subtle negative correlation was noted between the expression of the Con-A epitope and mannosidase expression. Our failure to identify additional enzymes might have resulted from the limited number of lectins available to us. In theory, other factors involved in biosynthetic pathways, such as factors involved in sugar-nucleotide biosynthesis or transport, could also regulate glycan expression on the cell surface.

Limitations of CIRES

Specific probes are unquestionably important for the successful application of CIRES. The most important aspect of lectin specificity is not affinity for the glycan ligand but rather the exclusivity of the enzyme. To calculate statistically significant correlations, a set of cell lines expressing different amounts of the target glycan should be used. The uniform expression of the target glycan in the cell set is undesirable.

To evaluate this methodology, we used the plant lectins that have been used extensively in other glycan studies. Since the correlations are identified by statistical calculations alone, we first assessed those lectins that had already been correlated with specific enzyme genes, to test for the identification of genes that matched glycan expression only by chance. Therefore, when CIRES is applied using uncharacterized glycan-binding probes, the bi-

ological relevance of the correlated genes must be confirmed by altering their expression in the cells. This requirement could be viewed as a limitation of the system. However, the alteration of target glycan expression has been an enduring and major objective of glycobiological experiments concerning lectins. As indicated in Figure 1, the CIRES methodology includes confirmation of the correlation by using glycan-related gene overexpression or silencing. Confirming biological relevance via the transfer of a correlated gene has the additional benefit of providing cells with a different expression level of the epitope of interest, which can be valuable for further assessment of lectin recognition in biological systems. Changing the cell surface expression of glycans for specific anti-glycan probes has been difficult, because the rate-limiting glycosyltransferase must be identified and overexpressed. Thus, allowing for a glycan-related gene transfer procedure that produces glycan-altered cells for further experiments is a major merit of the CIRES methodology.

CIRES alone cannot identify the specific glycan structure to which an anti-glycan probe binds; at the same time, knowledge of the structure of interest does not necessarily mean that modifying its expression on cells is possible. Using the CIRES method will likely result in the production of cells with modified glycan expression, but the actual structure bound by the probe may be unknown. This situation is somewhat similar to that of glycan-array binding studies, in which the probe that binds best on the glycan array does not necessarily bind the same glycan on the array as on cells and the identification of the glycan structure does not always result in the identification of the relevant biosynthetic enzyme. Thus, CIRES could be combined with conventional glycan-binding assays [44–46] to determine the specificity of glycan binding in a set of glycans and to identify the gene that modulates glycan expression on the cell surface, from among the pathway component enzymes. Thus, CIRES is a highly useful genetic strategy for studying the functionality of the interactions between glycans and glycan-binding proteins in cell-based systems.

MATERIALS AND METHODS

Reagents and cell culture

Two commercially available sets of biotin-conjugated plant lectins (Plant Lectin Set I and II) were obtained from Seikagaku (Tokyo, Japan). R-Phycoerythrin-conjugated streptavidin was obtained from Caltag (USA). The B-cell lines Daudi, Namalwa, Raji, Ramos, KMS-BM, and KMS-PE were obtained from the Japanese Collection of Research Bioresources and were cultured in RPMI 1640 medium supplemented with 10% fetal bovine serum, sodium pyruvate, non-essential amino acids, and 2-mercaptoethanol.

DNA microarrays

Gene expression profiling of the six B-cell lines was performed using a glycan-focused cDNA microarray (RIKEN human glycogene microarray, version 1) and a GEO Platform (GPL #3465) and compared with reference RNA (Clontech, USA) to create GEO Series GSE 4407, as reported elsewhere [11].

Flow cytometry

A total of 2.5×10^5 B cells in 100 μl FACS buffer (1% BSA and NaN_3 in PBS(−)) was incubated with excess biotinylated plant lectin probes at room temperature for 30 min. R-Phycoerythrin- or FITC-conjugated streptavidin was used to detect lectin binding. Data were obtained using FACScan or FACSCaliber (BD Biosciences, USA) and analyzed using FlowJo (Tristar, USA) or Cellquest software (BD Biosciences, USA). To cross-compare staining signals between cell lines, the mean fluorescence intensity (MFI) of the background staining was adjusted to around 10, and the relative staining signal was expressed as the ratio of sample MFI divided by the control MFI.

Statistical analysis

Fluorochrome signals on the microarray were acquired by an array scanner (Affymetrix 428) without background subtraction and were then background-corrected using a smoothing function [47]. They were then Lowess normalized using Linear Models for Microarray Data (LIMMA) [48] and the software program R [49]. Inter-array normalization was not used in cross-sample comparisons, as it seemed to cause over-normalization.

The signal from the B-cell lines was divided by the signal from the universal reference RNA [11] to obtain the relative expression profile for each gene in each cell line (Table S1). The gene expression profiles were compared with the lectin staining profiles obtained by flow cytometry. Similarities between the profiles were evaluated with Pearson's correlation coefficient, and probability values (P) were calculated using the correlation coefficient test. For a sample size of six, a correlation coefficient of 0.81 indicates a statistical significance level of 5%. The genes that correlated with lectin staining by this method were ranked according to correlation strength (Table S2), and this list was examined for genes that appeared to be relevant to previously reported lectin glycan epitopes and glycan biosynthetic pathways (Figure 1).

Retrovirus-mediated transduction of glycan-related genes

Retroviruses were prepared and were used to infect Namalwa cells, as reported previously [11]. Briefly, full-length glycosyltransferase cDNA was cloned into a modified MSCV vector, which expressed cDNA and EGFP via an internal ribosome entry site. The plasmid was transiently transfected into Plat-A packaging cells [50], and retrovirus-containing supernatants were collected. Namalwa cells were spin-infected (2000 rpm, 32°C, 120 min) with the retrovirus in the presence of 6 μg/ml polybrene.

The retrovirus-infected cells were cultured for 2 days after infection before analysis by flow cytometry. EGFP-positive and -negative cells were regarded as infected and non-infected cells, respectively. The staining of these two populations was used as the control.

Lectin blotting

B cells were sonicated in detergent-free lysis buffer [10 mM Tris-HCl (pH 7.6), 1 mM DTT, 1 mM EDTA, 0.25 M sucrose, and protease inhibitor cocktail (Roche)]. Postnuclear supernatants were further ultracentrifuged, and the pellets (membrane fraction) were resuspended in lysis buffer. The suspensions were subjected to lectin blotting with HRP-conjugated PHA-E4. The signal intensity was measured by exposure of the membrane to LAS300 (Fujifilm, Japan).

Sialidase treatment

Sialidase treatment was carried out as reported elsewhere [11]. Briefly, Daudi cells were incubated with sialidase in 100 mM sodium acetate (pH 5.2) at room temperature prior to lectin staining. Sialidases from *Arthrobacter ureafaciens* (AUS; Calbiochem, San Diego, USA) and *Salmonella typhimurium* (Takara, Kusatsu, Japan) were used.

SUPPORTING INFORMATION

Table S1 Complete gene expression profiles obtained from cDNA microarray: Fluorescent Cy3 (universal reference) and Cy5

(each Bcell line) readout data were acquired from the array scanner and following statistical calculations were applied using the software program R. First, background was corrected using "Edward method". Each data was then normalized using Linear Models for Microarray Data (LIMMA) to correct bias between fluorescent dyes. Finally, the Cy5 signal from the B cell lines was divided by the Cy3 signal to obtain the relative expression profile for each spot and resultant relative values were shown in columns I through N for each cells. Column A shows serial number of all spots on microarray and column B through E show physical location of all spots on glass slide-based cDNA microarray.
Found at: doi:10.1371/journal.pone.0001232.s001 (0.31 MB XLS)

Table S2 Lists of correlated genes with lectin staining: This is an Exel file consists of 14 worksheets. First sheet shows full list of genes spotted on the Glycan-focuesed microarray and their gene ID numbers. Following sheets are the lists of genes that exhibited stronger correlation with indicated lectin staining profiles. See "Materials and Methods" for the method applied for calculation.
Found at: doi:10.1371/journal.pone.0001232.s002 (0.40 MB XLS)

ACKNOWLEDGMENTS

The authors thank Dr. Hisashi Narimatsu (AIST) for full-length cDNA clones of glycosyltransferases and Dr. Toshio Kitamura (University of Tokyo) for Plat-A packaging cells. We also thank Drs. Atsushi Kuno (AIST) and Eiji Miyoshi (Osaka University) for helpful discussions about lectin determinants.

Author Contributions

Conceived and designed the experiments: HT YK HY AS YO. Performed the experiments: YN RF HY. Analyzed the data: HT YN RF HY YO GT. Contributed reagents/materials/analysis tools: HT YK AS YO GT. Wrote the paper: HT.

REFERENCES

1. Freeze HH (1999) Monosaccharide Metabolism In: Varki A, Cummings R, Esko JD, Freeze HH, Hart GW, Marth J, eds. Essentials of Glycobiology. New York: Cold Spring Harbor Laboratory Press. pp 69–84.
2. Hirschberg CB, Robbins PW, Abeijon C (1998) Transporters of nucleotide sugars, ATP, and nucleotide sulfate in the endoplasmic reticulum and Golgi apparatus Annu Rev Biochem 67: 49–69 9759482.
3. Kornfeld R, Kornfeld S (1985) Assembly of Asparagine-Linked Oligosaccharides Annu Rev Biochem 54: 631–664.
4. Aruffo A, Seed B (1987) Molecular cloning of a CD28 cDNA by a high-efficiency COS cell expression system Proc Natl Acad Sci U S A 84: 8573–7 2825196.
5. Seed B, Aruffo A (1987) Molecular cloning of the CD2 antigen, the T-cell erythrocyte receptor, by a rapid immunoselection procedure Proc Natl Acad Sci U S A 84: 3365–9 2437578.
6. Larsen RD, Rajan VP, Ruff MM, Kukowska-Latallo J, Cummings RD, et al. (1989) Isolation of a cDNA encoding a murine UDPgalactose:beta-D-galactosyl-1,4-N-acetyl-D-glucosaminide alpha-1,3-galactosyltransferase: expression cloning by gene transfer Proc Natl Acad Sci U S A 86: 8227–31 2510162.
7. Narimatsu H (2004) Construction of a human glycogene library and comprehensive functional analysis Glycoconj J 21: 17–24 15467393.
8. Comelli EM, Head SR, Gilmartin T, Whisenant T, Haslam SM, et al. (2006) A focused microarray approach to functional glycomics: transcriptional regulation of the glycome Glycobiology 16: 117–31 16237199.
9. Takematsu H, Kozutsumi Y (2007) DNA microarray in glycobiology In: Greet-Jan B, Lee YC, Suzuki A, Taniguchi N, Voragen AGJ, eds. Comprehensive Glycoscience vol. 2. Oxford: Elsevier. pp 428–448.
10. Kawano S, Hashimoto K, Miyama T, Goto S, Kanehisa M (2005) Prediction of glycan structures from gene expression data based on glycosyltransferase reactions Bioinformatics 21: 3976–82 16159923.
11. Naito Y, Takematsu H, Koyama S, Miyake S, Yamamoto H, et al. (2007) Germinal center marker GL7 probes activation-dependent repression of N-glycolylneuraminic acid, a sialic acid species involved in the negative modulation of B cell activation Mol Cell Biol 27: 3008–3022.
12. Fernandes B, Sagman U, Auger M, Demetrio M, Dennis JW (1991) Beta 1-6 branched oligosaccharides as a marker of tumor progression in human breast and colon neoplasia Cancer Res 51: 718–23 1985789.
13. Yamamoto H, Swoger J, Greene S, Saito T, Hurh J, et al. (2000) Beta1,6-N-acetylglucosamine-bearing N-glycans in human gliomas: implications for a role in regulating invasivity Cancer Res 60: 134–42 10646865.
14. Granovsky M, Fata J, Pawling J, Muller WJ, Khokha R, et al. (2000) Suppression of tumor growth and metastasis in Mgat5-deficient mice Nat Med 6: 306–12 10700233.
15. Partridge EA, Le Roy C, Di Guglielmo GM, Pawling J, Cheung P, et al. (2004) Regulation of cytokine receptors by Golgi N-glycan processing and endocytosis Science 306: 120–4 15459394.
16. Hennet T, Chui D, Paulson JC, Marth JD (1998) Immune regulation by the ST6Gal sialyltransferase Proc Natl Acad Sci U S A 95: 4504–9 9539767.
17. Kuno A, Uchiyama N, Koseki-Kuno S, Ebe Y, Takashima S, et al. (2005) Evanescent-field fluorescence-assisted lectin microarray: a new strategy for glycan profiling Nat Methods 2: 851–6 16278656.
18. Gillespie W, Paulson JC, Kelm S, Pang M, Baum LG (1993) Regulation of alpha 2,3-sialyltransferase expression correlates with conversion of peanut agglutinin (PNA)+ to PNA- phenotype in developing thymocytes J Biol Chem 268: 3801–4 8440675.
19. Priatel JJ, Chui D, Hiraoka N, Simmons CJ, Richardson KB, et al. (2000) The ST3Gal-I sialyltransferase controls CD8+ T lymphocyte homeostasis by modulating O-glycan biosynthesis Immunity 12: 273–83 10755614.
20. Kaifu R, Osawa T, Jeanloz RW (1975) Synthesis of 2-O-(2-acetamido-2-deoxy-beta-D-glucopyranosyl)-D-mannose, and its interaction with D-mannose-specific lectins Carbohydr Res 40: 111–7 1125946.
21. Shinkawa T, Nakamura K, Yamane N, Shoji-Hosaka E, Kanda Y, et al. (2003) The absence of fucose but not the presence of galactose or bisecting N-acetylglucosamine of human IgG1 complex-type oligosaccharides shows the critical role of enhancing antibody-dependent cellular cytotoxicity J Biol Chem 278: 3466–73 12427744.
22. Wang X, Inoue S, Gu J, Miyoshi E, Noda K, et al. (2005) Dysregulation of TGF-beta1 receptor activation leads to abnormal lung development and emphysema-like phenotype in core fucose-deficient mice Proc Natl Acad Sci U S A 102: 15791–6 16236725.
23. Matsumoto I, Osawa T (1969) Purification and characterization of an anti-H(O) phytohemagglutinin of Ulex europeus Biochim Biophys Acta 194: 180–9 5353123.
24. Okajima T, Fukumoto S, Miyazaki H, Ishida H, Kiso M, et al. (1999) Molecular cloning of a novel alpha2,3-sialyltransferase (ST3Gal VI) that sialylates type II lactosamine structures on glycoproteins and glycolipids J Biol Chem 274: 11479–86 10206952.
25. Ito N, Imai S, Haga S, Nagaike C, Morimura Y, et al. (1996) Localization of binding sites of Ulex europaeus I, Helix pomatia and Griffonia simplicifolia I-B4 lectins and analysis of their backbone structures by several glycosidases and poly-N-acetyllactosamine-specific lectins in human breast carcinomas Histochem Cell Biol 106: 331–9 8897074.
26. Furukawa K, Sato T (1999) Beta-1,4-galactosylation of N-glycans is a complex process Biochim Biophys Acta 1473: 54–66 10580129.
27. Crowley JF, Goldstein IJ, Arnarp J, Lonngren J (1984) Carbohydrate binding studies on the lectin from Datura stramonium seeds Arch Biochem Biophys 231: 524–33 6203486.
28. Yamashita K, Totani K, Ohkura T, Takasaki S, Goldstein IJ, et al. (1987) Carbohydrate binding properties of complex-type oligosaccharides on immobilized Datura stramonium lectin J Biol Chem 262: 1602–7 3805046.
29. Ihara Y, Nishikawa A, Taniguchi N (1995) Effects of dibutyryl cAMP and bromodeoxyuridine on expression of N-acetylglucosaminyltransferases III and V in GOTO neuroblastoma cells Glycoconj J 12: 787–94 8748156.
30. Sasai K, Ikeda Y, Eguchi H, Tsuda T, Honke K, et al. (2002) The action of N-acetylglucosaminyltransferase-V is prevented by the bisecting GlcNAc residue at the catalytic step FEBS Lett 522: 151–5 12095636.
31. Miyoshi E, Nishikawa A, Ihara Y, Hayashi N, Fusamoto H, et al. (1994) Selective suppression of N-acetylglucosaminyltransferase III activity in a human hepatoblastoma cell line transfected with hepatitis B virus Cancer Res 54: 1854–8 8137300.
32. Sultan AS, Miyoshi E, Ihara Y, Nishikawa A, Tsukada Y, et al. (1997) Bisecting GlcNAc structures act as negative sorting signals for cell surface glycoproteins in forskolin-treated rat hepatoma cells J Biol Chem 272: 2866–72 9006930.
33. Wang WC, Cummings RD (1988) The immobilized leukoagglutinin from the seeds of Maackia amurensis binds with high affinity to complex-type Asn-linked oligosaccharides containing terminal sialic acid-linked alpha-2,3 to penultimate galactose residues J Biol Chem 263: 4576–85 3350806.
34. Konami Y, Yamamoto K, Osawa T, Irimura T (1994) Strong affinity of Maackia amurensis hemagglutinin (MAH) for sialic acid-containing Ser/Thr-linked carbohydrate chains of N-terminal octapeptides from human glycophorin A FEBS Lett 342: 334–8 8150094.
35. Knibbs RN, Goldstein IJ, Ratcliffe RM, Shibuya N (1991) Characterization of the carbohydrate binding specificity of the leukoagglutinating lectin from Maackia amurensis. Comparison with other sialic acid-specific lectins J Biol Chem 266: 83–8 1985926.

36. Stanley P, Caillibot V, Siminovitch L (1975) Selection and characterization of eight phenotypically distinct lines of lectin-resistant Chinese hamster ovary cell Cell 6: 121–8 1182798.
37. Kitagawa H, Paulson JC (1994) Differential expression of five sialyltransferase genes in human tissues J Biol Chem 269: 17872–8 8027041.
38. Bierhuizen MF, Mattei MG, Fukuda M (1993) Expression of the developmental I antigen by a cloned human cDNA encoding a member of a beta-1,6-N-acetylglucosaminyltransferase gene family Genes Dev 7: 468–78 8449405.
39. Moremen KW (2002) Golgi alpha-mannosidase II deficiency in vertebrate systems: implications for asparagine-linked oligosaccharide processing in mammals Biochim Biophys Acta 1573: 225–35 12417404.
40. Chen Y, Jain RK, Chandrasekaran EV, Matta KL (1995) Use of sialylated or sulfated derivatives and acrylamide copolymers of Gal beta 1,3GalNAc alpha- and GalNAc alpha- to determine the specificities of blood group T- and Tn-specific lectins and the copolymers to measure anti-T and anti-Tn antibody levels in cancer patients Glycoconj J 12: 55–62 7795413.
41. Nakamura-Tsuruta S, Kominami J, Kuno A, Hirabayashi J (2006) Evidence that Agaricus bisporus agglutinin (ABA) has dual sugar-binding specificity Biochem Biophys Res Commun 347: 215–20 16824489.
42. Hakomori S (2004) Carbohydrate-to-carbohydrate interaction in basic cell biology: a brief overview Arch Biochem Biophys 426: 173–81 15158668.
43. Paulson JC, Blixt O, Collins BE (2006) Sweet spots in functional glycomics Nat Chem Biol 2: 238–48 16619023.
44. Fukui S, Feizi T, Galustian C, Lawson AM, Chai W (2002) Oligosaccharide microarrays for high-throughput detection and specificity assignments of carbohydrate-protein interactions Nat Biotechnol 20: 1011–7 12219077.
45. Blixt O, Head S, Mondala T, Scanlan C, Huflejt ME, et al. (2004) Printed covalent glycan array for ligand profiling of diverse glycan binding proteins Proc Natl Acad Sci U S A 101: 17033–8 15563589.
46. Kamekawa N, Hayama K, Nakamura-Tsuruta S, Kuno A, Hirabayashi J (2006) A combined strategy for glycan profiling: a model study with pyridylaminated oligosaccharides J Biochem (Tokyo) 140: 337–47 16861248.
47. Edwards D (2003) Non-linear normalization and background correction in one-channel cDNA microarray studies Bioinformatics 19: 825–33 12724292.
48. Smyth GK (2005) Limma: linear models for microarray data. In: R. Gentleman VC, S. Dudoit, R. Irizarry, W. Huber, eds. 'Bioinformatics and Computational Biology Solutions using R and Bioconductor'. New York: Springer. pp Chapter 23.
49. Team RDC (2004) R: A Language and Environment for Statistical Computing. Vienna: R Foundation for Statistical Computing, http://www.R-project.org.
50. Morita S, Kojima T, Kitamura T (2000) Plat-E: An efficient and stable system for transient packaging of retroviruses Gene Ther 7: 1063–6 10871756.
51. Cummings R (1999) Plant Lectins. In: Varki A, Cummings R, Esko JD, Freeze HH, Hart GW, Marth J. Essentials of Glycobiology. New York: Cold Spring Harbor Laboratory Press. pp 455–468.

Available online at www.sciencedirect.com
ScienceDirect
Biochemical and Biophysical Research Communications 363 (2007) 835–839
BBRC
www.elsevier.com/locate/ybbrc

Abnormal features in mutant cerebellar Purkinje cells lacking junctophilins

Atsushi Ikeda [a,1], Taisuke Miyazaki [b,1], Sho Kakizawa [c], Yasushi Okuno [d], Soken Tsuchiya [d], Akira Myomoto [d], Shin-ya Saito [e], Tetsuji Yamamoto [a], Tetsuo Yamazaki [a], Masamitsu Iino [c], Gozoh Tsujimoto [d], Masahiko Watanabe [b], Hiroshi Takeshima [a,e,*]

[a] Department of Biological Chemistry, Graduate School of Pharmaceutical Sciences, Kyoto University, Kyoto 606-8501, Japan
[b] Department of Anatomy, Hokkaido University Graduate School of Medicine, Sapporo, Japan
[c] Department of Pharmacology, Graduate School of Medicine, The University of Tokyo, Tokyo, Japan
[d] Department of Genomic Drug Discovery Science, Graduate School of Pharmaceutical Sciences, Kyoto University, Kyoto 606-8501, Japan
[e] Department of Medical Chemistry, Tohoku University Graduate School of Medicine, Sendai, Japan

Received 1 September 2007
Available online 24 September 2007

Abstract

Junctional membrane complexes (JMCs) generated by junctophilins are required for Ca^{2+}-mediated communication between cell-surface and intracellular channels in excitable cells. Knockout mice lacking neural junctophilins (JP-DKO) show severe motor defects and irregular cerebellar plasticity due to abolished channel crosstalk in Purkinje cells (PCs). To precisely understand aberrations in JP-DKO mice, we further analyzed the mutant PCs. During the induction of cerebellar plasticity via electrical stimuli, JP-DKO PCs showed insufficient depolarizing responses. Immunochemistry detected mild impairment in synaptic maturation and hyperphosphorylation of protein kinase Cγ in JP-DKO PCs. Moreover, gene expression was slightly altered in the JP-DKO cerebellum. Therefore, the mutant PCs bear marginal but widespread abnormalities, all of which likely cause cerebellar motor defects in JP-DKO mice.

Keywords: Long-term depression; Multiple innervation; Protein kinase C; Ryanodine receptor

Functional communications between cell-surface and intracellular channels play indispensable roles in excitable cells [1]. Ca^{2+}-mediated channel crosstalk often takes place in specific subcellular structures, called the junctional membrane complexes (JMCs), which are characterized by close apposition of the endoplasmic/sarcoplasmic reticulum (ER/SR) and the cell membrane [2]. Of four junctophilin (JP) subtypes, JP1 and JP2 contribute to the formation of JMCs in striated muscle [3–5], while JP3 and JP4 are co-expressed in neuron [6]. Double-knockout mice deficient for both neural JPs (JP-DKO) exhibit impaired motor coordination and learning [7]. In cerebellar Purkinje cells (PCs), the generation of slow afterhyperpolarization (sAHP) following the climbing fiber (CF)-mediated complex spike requires Ca^{2+}-mediated channel crosstalk between P/Q-type voltage-gated Ca^{2+} channels (P/Q channels), ryanodine receptor channels (RyRs) and small-conductance Ca^{2+}-activated K^+ channels (SK channels). This channel communication probably occurs in JP-mediated JMCs and is indispensable for long-term depression (LTD) at parallel fiber (PF)-PC synapses. Indeed, this channel crosstalk is severely impaired and an LTD-inducing paradigm adversely leads to long-term potentiation

* Corresponding author. Address: Department of Biological Chemistry, Graduate School of Pharmaceutical Sciences, Kyoto University, Kyoto 606-8501, Japan. Fax: +81 75 753 4605.
E-mail address: takeshim@pharm.kyoto-u.ac.jp (H. Takeshima).
[1] These authors contributed equally to this work.

0006-291X/$ - see front matter © 2007 Elsevier Inc. All rights reserved.
doi:10.1016/j.bbrc.2007.09.062

(LTP) in JP-DKO PCs [7]. In our continuing attempt to deepen understanding of impaired cerebellar functions in JP-DKO mice, we report irregular PC excitability, atypical CF-wiring to PCs, hyperphosphorylation of protein kinase C (PKC) and altered gene expression.

Materials and methods

Electrophysiological measurements. JP-3(−/−) JP-4(−/−) mice (JP-DKO) and JP-3(+/−) JP-4(+/−) mice (JP-DHE) were described previously [8]. For electrophysiological measurements, cerebellar slices were prepared from mice aged 8–10 weeks and whole-cell recordings were performed from PCs [7,9]. LTD was induced by conjunctive stimulation (CJS, 300 single PF stimuli in conjunction with single CF stimuli repeated at 1 Hz for 5 min) after the initial baseline recording for at least 10 min.

Morphological analysis. Morphological analyses were carried out using mice aged 6–10 weeks [10,11]. For anterograde labeling of CFs, the inferior olive in the anesthetized mice were injected with dextran Texas red. After 4 days of survival, mice were fixed by transcardial perfusion, and prepared microslicer sections were immunostained for calbindin and vesicular glutamate transporter type 2 (VGluT2) and analyzed using a confocal microscope.

Microarray, real-time PCR and immunoblot analyses. Total RNA was isolated from the cerebella of male mice aged 6–8 weeks using the Isogen reagent (Nippongene, Japan), fluorescence labeled and hybridized onto the Mouse Genome 430 2.0 Array (Affymetrix). Raw data obtained were analyzed as described previously [12]. Real-time PCR was performed using the Chromo 4 system (Bio-Rad). Cerebellar homogenates were examined by immunoblotting [10] using the following antibodies: total and phosphorylated (p) PKCγ, PDE (phosphodiesterase) 1C (Abcam), pPKCα, pMARCKS (myristoylated alanine-rich C kinase substrate), pNR1 (N-methyl-D-aspartate receptor 1), pGluR1 (glutamate receptor 1), pCREB (cAMP response element-binding protein), pDARPP (Dopamine- and cAMP-regulated neuronal phosphoprotein), Nab2 (Ngfi-A binding protein 2) (Millipore), pERK1/2 (extracellular signal-regulated kinase 1/2), Egr1 (early growth response 1) (Cell Signaling), β-tubulin (Sigma), and pCaMKII (Ca^{2+}/calmodulin-dependent protein kinase II, gift from Dr. Fukunaga, Tohoku University, Japan).

Results and discussion

Atypical depolarizing responses in JP-DKO PCs

In cerebellar slice preparations, CJS to both PF and CF induces LTD at PF-PC synapses [13]. In control mice, PF-evoked excitatory postsynaptic currents (PF-EPSCs) recorded in voltage-clamped PCs were remarkably decreased from the baseline level after CJS. As shown in Fig. 1A and B, this LTD-inducing paradigm adversely led to LTP in JP-DKO slices and control slices treated with apamin, an SK channel inhibitor. It has been reported that PF-LTP is induced by CJS when LTD was previously established at the CF-PC synapse [14] and also that both CF-evoked spikelets and dendritic Ca^{2+} transients are weakened in PCs after the induction of CF-LTD [15]. Based on these findings, we focused on CF-evoked spikelets in JP-DKO PCs. During CJS composed of stimuli repeated 300 times, control PCs showed constant voltage responses of spikelets, whereas spikelet numbers were significantly decreased at the late phase in both JP-DKO and apamin-treated control PCs (Fig. 1C and D). Therefore, the reverse plasticity in JP-DKO and the apamin-treated PCs may be cardinally induced by the impaired spikelets due to insufficient SK channel opening.

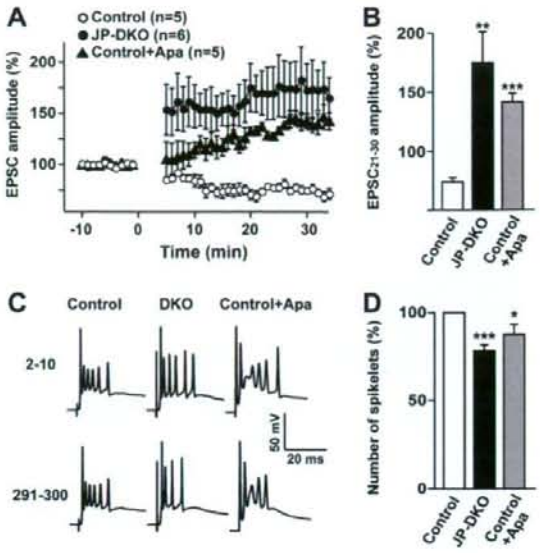

Fig. 1. Deformed spikelets during CJS in JP-DKO and apamin-treated control PCs. (A) PF-EPSCs were normalized by the mean value observed before CJS. Apamin (Apa; 200 nM) was applied to the bathing solution during recording. (B) Average EPSP amplitude during the 21–30 min period after CJS. (C) Representative voltage responses of PCs at early (2–10) and late (291–300) phases during CJS. (D) Averaged spikelet numbers at 291–300th responses normalized by values at 2–10th responses. Data are presented as means ± SEM ($^{*}p < 0.05$, $^{**}p < 0.01$ and $^{***}p < 0.001$ in *t*-test).

In PCs, P/Q channels, rather than voltage-gated Na^{+} channels, predominantly contribute to the generation of the slow spikelets [16]. JP-mediated channel crosstalk between P/Q channels, RyRs, and SK channels generates sAHP following spikelets [7]. Voltage-gated channels incorporate voltage-dependent inactivation features and their recovery from inactivated states requires the repolarization of the membrane potential. As a predicted mechanism underlying the reverse plasticity, sAHP deficiency may prevent the recovery of P/Q channels from the inactivated state and likely weakens spikelets during CJS in both JP-DKO and the apamin-treated PCs. JP-DKO and the apamin-treated PCs showed slight differences in the temporal profile of PF-EPSC potentiation (Fig. 1A). In particular, obvious differences observed immediately after CJS may imply as-yet-unrecognized defects in JP-DKO PCs besides sAHP deficiency due to SK channel dysfunctioning.

Mild disturbance in CF innervation to JP-DKO PCs

In our previous report, PF-PC synapses appeared normal in JP-DKO mice. To morphologically analyze the physical connection between CFs and PCs, CFs were anterogradely labeled (aCF) with dextran Texas red; CF-PC synapses and PC dendrites were visualized with antibodies

against VGluT2 and calbindin, respectively. In control mice (Fig. 2A), aCF precisely followed the branching of PC shaft dendrites and the terminal swellings of aCF overlapped completely with VGluT2. The DKO cerebellum showed no gross morphological abnormalities; PC dendrites were well branched and associated with CF terminals in regular spacing (Fig. 2B1). However, when carefully observed at higher magnifications, the same dendritic shaft innervated by aCF terminals (red arrows) was associated with a few synaptic terminals of tracer-unlabeled CFs (uCF, green arrows) (Fig. 2B2–5). This mild type of multiple CF innervation was often observed in the DKO cerebellum by this anatomical analysis, but was under the detection threshold by electrophysiological analysis [7].

In recent studies, a close correlation between multiple CF innervation and motor discoordination was repeatedly appreciated in a number of knockout mice including mutant mice defective in P/Q channels [11] and PKCγ [17]. Thus, the mild multiple innervation, together with the deranged Ca^{2+}-mediated channel crosstalk [7], may lead to severe motor discoordination in JP-DKO mice. The predominant distribution of JPs to the somatodendritic regions of PCs [6] suggests that PCs, rather than CFs, are likely responsible for the retention of the aberrant CF-PC innervation in adult JP-DKO mice. Because both P/Q channels and PKCγ in PCs are essential for eliminating excess CF-PC synapses, two possibilities are reasonably proposed behind the mild symptom in JP-DKO PCs, i.e., the reduction of P/Q channel-mediated Ca^{2+} influx during repeated depolarization and the predicted hyperactivation of PKCγ (see below).

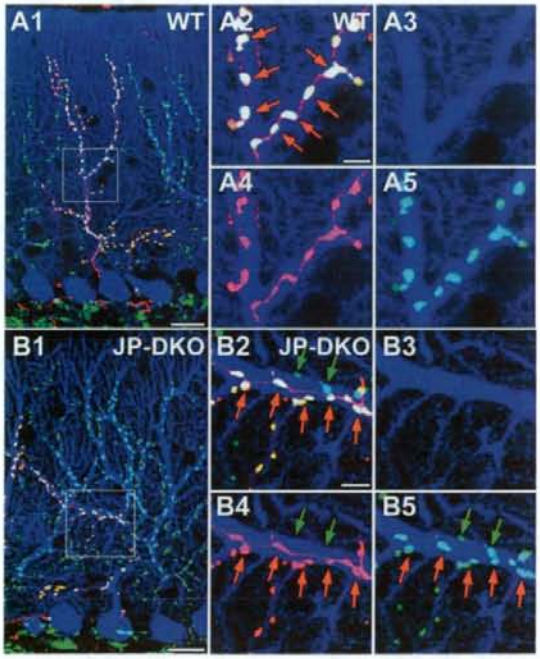

Fig. 2. Aberrant CF-PC innervation in JP-DKO cerebellum. Cerebellar sections were labeled for calbindin (blue), VGluT2 (green) and the anterograde CF tracer dextran Texas red (red) in control (A) and JP-DKO mice (B). Boxed regions in A1 and B1 are magnified in A2–5 and B2–5, respectively. The arrows indicate terminals of anterogradely-labeled CFs (aCF, red arrows) and unlabeled CFs (uCF, green arrows), respectively. Scale bars, 20 μm in A1 and B1; 5 μm in A2–5 and B2–5.

Hyperphosphorylation of PKCγ in JP-DKO PCs

Ca^{2+}-dependent signaling plays a central role for inducing synaptic plasticity such as cerebellar LTD and hippocampal LTP [13]. In our immunoblot analysis, the JP-DKO cerebellum showed an enhanced phosphorylation level at T674 of PKCγ without affecting other phosphorylation sites or its protein content (Fig. 3 and Suppl. Fig. 1). In addition, we did not detect any abnormalities in phosphorylation of well-known PKC substrates (MARCKS and NR1) or of other protein kinases. Since PKCγ is predominantly expressed in PCs among cerebellar cell types, the hyperphosphorylation seems to occur in JP-DKO PCs. Although we have observed regular CF-mediated Ca^{2+} responses in JP-DKO PC soma regions [7], sAHP deficiency could slightly prolong opening of P/Q channels upon sporadic stimuli. It might be that enhanced Ca^{2+} signaling at the microdomain level stimulates the autophosphorylation of PKCγ in JP-DKO PCs under basal conditions. In addition to facilitated autophosphorylation, PKCγ activation accompanies its translocation to the cell membrane from the cytoplasm. PKCγ was clearly detected in the cytoplasm and on the cell membrane, and no difference was observed in its subcellular localization between control and JP-DKO PCs (Suppl. Fig. 2). Although MARCKS and NR1 showed normal phosphorylation levels, it is still possible that PKCγ activity was enhanced to change phosphorylation states of unknown signaling molecules regulating cerebellar motor functions in JP-DKO PCs. On the other hand, PKCγ-knockout mice suffering severe multiple innervation have established its essential

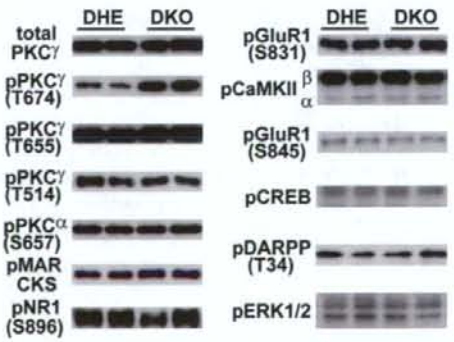

Fig. 3. Hyperphosphorylation at T674 of PKCγ in JP-DKO cerebellum. Representative immunoblot data are shown. The immunoreactivities were statistically analyzed in Suppl. Fig. 1.

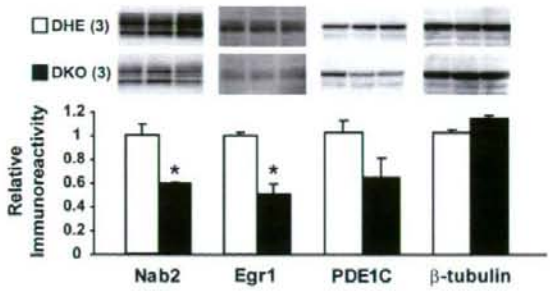

Fig. 4. Reduced expression of Nab2 and Egr1 in JP-DKO cerebellum. Immunoreactivities (upper images) were statistically analyzed. Data are presented as means ± SEM (n values in parentheses, $^*p < 0.05$ in t-test).

role in CF-PC synaptic maturation [17]. Hyperphosphorylated PKCγ might also affect signaling processes for CF elimination in JP-DKO PCs.

Altered gene expression in JP-DKO cerebellum

We finally surveyed altered gene expression in the JP-DKO cerebellum. Our microarray analysis suggested minimally altered gene expression between genotypes (Suppl. Fig. 3), but identified eight up-regulated and three down-regulated candidate genes in JP-DKO mice (Suppl. Table 1). Of the candidates, the down-regulation of *Nab2* was confirmed by real-time PCR and immunoblotting (Fig. 4 and Suppl. Fig. 4). Nab2 is a transcriptional corepressor induced by the zinc-finger transcription factor Egr1, which is up-regulated by neuronal stimuli and essential for LTP in hippocampal neurons [18]. In the JP-DKO cerebellum, Egr1 protein was obviously decreased (Fig. 4). The reduced Nab2 and Egr1 levels may be due to less electrically-active properties in JP-DKO PCs exhibiting the impaired spikelets (Fig. 1).

Although we need to examine the precise linkage between JP deficiency and several abnormalities reported here, they may be directly or indirectly connected with sAHP deficiency in JP-DKO PCs as discussed above. These chronic abnormalities observed under normal housing conditions likely further aggravate weakened spikelets caused by the sAHP deficiency to produce the severity of the reverse plasticity in the JP-DKO cerebellum. Our previous study suggests impairments of overall brain functions, including the salivary reflex and hippocampus-dependent memory in JP-DKO mice [8]. The presented data clearly suggest that JP-mediated JMCs are essential for a broad range of cellular homeostasis in various neurons.

Acknowledgments

This work was supported in part by grants from the Ministry of Education, Culture, Sports, Science, and Technology of Japan, the Naito Foundation, the Sumitomo Foundation, the Uehara Memorial Foundation, the Life Science Foundation, and the Takeda Science Foundation.

Appendix A. Supplementary data

Supplementary data associated with this article can be found, in the online version, at doi:10.1016/j.bbrc.2007.09.062.

References

[1] M.J. Berridge, M.D. Bootman, H.L. Roderick, Calcium signalling: dynamics, homeostasis and remodeling, Nat. Rev. Mol. Cell. Biol. 4 (2003) 517–529.
[2] A. Divet, S. Paesante, C. Bleunven, A. Anderson, S. Treves, F. Zorzato, Novel sarco(endo)plasmic reticulum proteins and calcium homeostasis in striated muscles, J. Muscle Res. Cell Motil. 26 (2005) 7–12.
[3] H. Takeshima, S. Komazaki, M. Nishi, M. Iino, K. Kangawa, Junctophilins: a novel family of junctional membrane complex proteins, Mol. Cell 6 (2000) 11–22.
[4] K. Ito, S. Komazaki, K. Sasamoto, M. Yoshida, M. Nishi, K. Kitamura, H. Takeshima, Deficiency of triad junction and contraction in mutant skeletal muscle lacking junctophilin type 1, J. Cell Biol. 154 (2001) 1059–1068.
[5] S. Komazaki, M. Nishi, H. Takeshima, Abnormal junctional membrane structures in cardiac myocytes expressing ectopic junctophilin type 1, FEBS Lett. 542 (2003) 69–73.
[6] M. Nishi, H. Sakagami, S. Komazaki, H. Kondo, H. Takeshima, Coexpression of junctophilin type 3 and type 4 in brain, Mol. Brain Res. 110 (2003) 102–110.
[7] S. Kakizawa, Y. Kishimoto, K. Hashimoto, T. Miyazaki, K. Furutani, H. Shimizu, M. Fukaya, M. Nishi, H. Sakagami, A. Ikeda, H. Kondo, M. Kano, M. Watanabe, M. Iino, H. Takeshima, Junctophilin-mediated channel crosstalk essential for cerebellar synaptic plasticity, EMBO J. 26 (2007) 1924–1933.
[8] S. Moriguchi, M. Nishi, S. Komazaki, H. Sakagami, T. Miyazaki, H. Masumiya, S. Saito, M. Watanabe, H. Kondo, H. Yawo, K. Fukunaga, H. Takeshima, Functional uncoupling between Ca^{2+} release and afterhyperpolarization in mutant hippocampal neurons lacking junctophilins, Proc. Natl. Acad. Sci. USA 103 (2006) 10811–10816.
[9] S. Kakizawa, T. Miyazaki, D. Yanagihara, M. Iino, M. Watanabe, M. Kano, Maintenance of presynaptic function by AMPA receptor-mediated excitatory postsynaptic activity in adult brain, Proc. Natl. Acad. Sci. USA 102 (2005) 19180–19185.
[10] T. Miyazaki, K. Hashimoto, A. Uda, H. Sakagami, Y. Nakamura, S. Saito, M. Nishi, H. Kume, A. Tohgo, I. Kaneko, H. Kondo, K. Fukunaga, M. Kano, M. Watanabe, H. Takeshima, Disturbance of cerebellar synaptic maturation in mutant mice lacking BSRPs, a novel brain-specific receptor-like protein family, FEBS Lett. 580 (2006) 4057–4064.
[11] T. Miyazaki, K. Hashimoto, H.S. Shin, M. Kano, M. Watanabe, P/Q-type Ca^{2+} channel alpha 1A regulates synaptic competition on developing cerebellar Purkinje cells, J. Neurosci. 24 (2004) 1734–1743.
[12] R.A. Irizarry, B.M. Bolstad, F. Collin, L.M. Cope, B. Hobbs, T.P. Speed, Summaries of Affymetrix GeneChip probe level data, Nucleic Acids Res. 31 (2003) e15.
[13] M. Ito, Cerebellar circuitry as a neuronal machine, Prog. Neurobiol. 78 (2006) 272–303.
[14] M. Coesmans, J.T. Weber, C.I. De Zeeuw, C. Hansel, Bidirectional parallel fiber plasticity in the cerebellum under climbing fiber control, Neuron 44 (2004) 691–700.
[15] J.T. Weber, C.I. De Zeeuw, D.J. Linden, C. Hansel, Long-term depression of climbing fiber-evoked calcium transients in

Purkinje cell dendrites, Proc. Natl. Acad. Sci. USA 100 (2003) 2878–2883.
[16] M.T. Schmolesky, J.T. Weber, C.I. De Zeeuw, C. Hansel, The making of a complex spike: ionic composition and plasticity, Annu. N. Y. Acad. Sci. 978 (2002) 359–390.
[17] M. Kano, K. Hashimoto, C. Chen, A. Abeliovich, A. Aiba, H. Kurihara, M. Watanabe, Y. Inoue, S. Tonegawa, Impaired synapse elimination during cerebellar development in PKCγ mutant mice, Cell 83 (1995) 1223–1231.
[18] M.W. Jones, M.L. Errington, P.J. French, A. Fine, T.V. Bliss, S. Garel, P. Charnay, B. Bozon, S. Laroche, S. Davis, A requirement for the immediate early gene Zif268 in the expression of late LTP and long-term memories, Nat. Neurosci. 4 (2001) 289–296.

Available online at www.sciencedirect.com
ScienceDirect
Biochemical and Biophysical Research Communications 362 (2007) 971–975
BBRC
www.elsevier.com/locate/ybbrc

Augmentation of drug-induced cell death by ER protein BRI3BP

Tetsuo Yamazaki [a,b,*], Nozomi Sasaki [a,b], Miyuki Nishi [b], Daiju Yamazaki [b], Atsushi Ikeda [b], Yasushi Okuno [c], Shinji Komazaki [d], Hiroshi Takeshima [b]

[a] *The 21st Century Center of Excellence Program, Tohoku University Graduate School of Medicine, Sendai 980-8575, Japan*
[b] *Department of Biological Chemistry, Graduate School of Pharmaceutical Sciences, Kyoto University, Kyoto 606-8501, Japan*
[c] *Department of Genomic Drug Discovery Science, Graduate School of Pharmaceutical Sciences, Kyoto University, Kyoto 606-8501, Japan*
[d] *Department of Anatomy, Saitama Medical University, Saitama 350-0495, Japan*

Received 14 August 2007
Available online 27 August 2007

Abstract

To determine the contribution of the endoplasmic reticulum (ER) to cell fate decision, we focused on BRI3-binding protein (BRI3BP) residing in this organelle. BRI3BP, when overexpressed, augmented the apoptosis of human embryonic kidney 293T cells challenged with drugs including the anti-cancer agent etoposide. In contrast, the knockdown of BRI3BP reduced the drug-triggered apoptosis. BRI3BP overexpression enhanced both mitochondrial cytochrome *c* release and caspase-3 activity in etoposide-treated cells. In response to etoposide, the ER reorganized into irregularly shaped lamellae in mock-transfected cells, whereas in BRI3BP-overexpressing cells, such reorganization was not observed. These observations suggest that BRI3BP is involved in the structural dynamics of the ER and affects mitochondrial viability. Taken together, BRI3BP, widely expressed in animal cell types, seems to possess a pro-apoptotic property and can potentiate drug-induced apoptosis.

Keywords: Apoptosis; Cytochrome *c*; Endoplasmic reticulum; Etoposide; BRI3BP; Mitochondria

The endoplasmic reticulum (ER) is a multifaceted organelle. It plays a major role in protein synthesis, folding and processing. In addition to its housekeeping functions, the ER emits signals to maintain cellular homeostasis. The accumulation of structurally defective proteins in the ER initiates stress responses, which are collectively referred to as the "unfolded protein response (UPR)" [1,2]. By enhancing the ERs capacity to refold and degrade aberrant proteins, the UPR initially operates in favor of cellular survival. In contrast, cell death is induced by the UPR when the cells are exposed to excessive and prolonged ER stress. The importance of the stress response has been demonstrated also in the pathogenesis of various diseases including ischemic/reperfusion injury, neurodegenerative diseases and diabetes [3]. Toward a better understanding of such pathophysiological signals, it is necessary to identify and characterize the signaling proteins transmitting ER information to the cytoplasm.

In this work, we focused on an ER-resident protein, BRI3-binding protein (BRI3BP) [4,5]. On the basis of the results obtained, we propose that BRI3BP contributes to cell fate decision by mediating joint activities between the ER and mitochondria.

Methods

Transfection and pharmacological treatment. Human embryonic kidney 293T (293T) cells were grown in DMEM (WAKO, Tokyo, Japan) supplemented with 10% fetal calf serum (FCS) at 37 °C in a 5% CO_2 humidified incubator. For overexpression, the cDNA fragment encoding human BRI3BP or murine calumin was PCR-generated and cloned in frame into the pcDNA4/myc-His vector (Invitrogen). The pcDNA4/myc-His/lacZ vector coding for β-galactosidase was obtained from Clontech Inc. The cells were plated 16 h prior to transfection in 12-well plates at

* Corresponding author. Address: Department of Biological Chemistry, Graduate School of Pharmaceutical Sciences, Kyoto University, Kyoto 606-8501, Japan. Fax: +81 75 753 4605.
E-mail address: yamazakt@pharm.kyoto-u.ac.jp (T. Yamazaki).

0006-291X/$ - see front matter © 2007 Elsevier Inc. All rights reserved.
doi:10.1016/j.bbrc.2007.08.082

1×10^5 cells per well. The expression construct was transfected into the cells using Lipofectamine 2000 (Invitrogen). At 30 h posttransfection, etoposide (Etop), thapsigargin (Tg), and tunicamycin (Tu) (all from WAKO) were added to the culture medium. The cells were incubated for a further 40 h and then examined flow cytometrically. For BRI3BP depletion, the following small interfering RNA (siRNA) duplex obtained from Dharmacon was transfected into 293T cells using X-tremeGENE siRNA transfection reagent (Roche): 5′-gcucuuggauguucuuggauu-3′ and 5′-uccaagaacauccaagagcuu-3′. Depletion of BRI3BP mRNA was confirmed by reverse transcription polymerase chain reaction (RT-PCR) using cDNAs, synthesized with PrimeScript reverse transcriptase (Takara Bio, Shiga, Japan), as templates. The following primers were used: for BRI3BP, 5′-GCGTCGACACCATGGGCGCGCGCCTCAGGCGGGC-3′ and 5′-GCGAATTCTACTTGTCCTTGGAGCGGTCCAGGCTC-3′, and for β-actin, 5′-GCATTGCTGACAGGATGCAG-3′ and 5′-CCTGCTTGCTGATCCACATC-3′. The siRNA-transfected cells were split onto another 12-well plate at 72 h posttransfection. After 16 h, the cells were chemically challenged as descried above and analyzed.

Cell viability and caspase-3 activity assay. Cell viability was determined as described previously [6]. To examine caspase-3 activation, the transfected cells were treated with either dimethyl sulfoxide (vehicle) or Etop in the presence or absence of the cell-permeable pan-caspase inhibitor Z-VAD-fmk (BD Bioscience). Subsequently, caspase-3 activity was measured by flow cytometry using the CaspGLOW fluorescein active capase-3 staining kit (Medical & Biological Lab., Nagano, Japan) according to the manufacturer's instructions.

Mitochondrial cytochrome c release and transmembrane potential. Mitochondrial cytochrome *c* content was measured as described previously [7], except that the secondary antibody used was coupled with Alexa Fluor 488 instead of phycoerythrin. For examining the mitochondrial membrane potential, pharmacologically treated 293T cells were incubated for 30 min with DMEM supplemented with 10% FCS and 1 μg/ml rhodamine 123 (Rh123) in a 5% CO_2 humidified incubator, washed with PBS, and subjected to flow cytometry.

Immunoblotting. For the immunoblotting of whole cell lysates, transfected 293T cells were lyzed at 24 h posttransfection in RIPA buffer (10 mM Tris–HCl (pH 7.6), 150 mM NaCl, 2 mM EDTA, 1% Triton X-100 and 1% sodium deoxycholate, protease inhibitor cocktail (Nacalai Tesque, Tokyo, Japan)). The antibodies against the following proteins were used: BAK, BAX, Bcl-2, Bcl-X_L and actin (Santa Cruz Biotech.), and GRP78 (Abcam). BRI3BP antiserum was produced by injecting rabbits with a glutathione *S*-transferase fusion protein containing amino acids 203–253 of murine BRI3BP.

Ultrastructural analysis. The pharmacologically treated cells were prepared for electron microscopy study as described previously [8].

Statistics. Statistical significance was evaluated using Student's *t* test unless otherwise mentioned.

Results

Facilitation of drug-induced apoptosis by BRI3BP overexpression

The localization of BRI3BP to both the ER and the nuclear membrane prompted us to explore the possibility that BRI3BP is involved in signaling from the ER. To this end, 293T cells transfected with human BRI3BP that was fused to the mycHis tag (Suppl. Fig. 1A and B) were incubated with apoptosis inducers including ER stressors such as Tg (sarcoplasmic/endoplasmic Ca^{2+}–ATPase inhibitor) and Tu (*N*-glycosylation inhibitor), and the chemotherapy drug Etop (topoisomerase II inhibitor). The cells were probed using a combination of fluorescein isothiocyanate-coupled Annexin V (Annexin V-FITC) and the DNA-specific fluorochrome 7-amino-actinomycin D (7-AAD) to simultaneously determine phosphatidyl serine exposure and plasma membrane permeability by flow cytometry [9,10]. Subsequently, cell subsets undergoing early (Annexin V^+/7-AAD^-) and late (Annexin V^+/7-AAD^+) apoptosis were quantified (Suppl. Fig. 1C). BRI3BP transfection led to a 15–30% increase in apoptosis compared with mock transfection. On the other hand, no obvious effects of β-galactosidase (cytosolic protein) and calumin (ER transmembrane protein [6]) on apoptosis were detected (Suppl. Fig. 1D), suggesting that BRI3BP specifically enhances drug-initiated apoptosis. Increased vulnerability to the pharmacological insults was corroborated over a wide range of drug concentrations (Fig. 1A).

Reduction of drug-induced apoptosis by BRI3BP depletion

We further investigated the role of BRI3BP using an siRNA-mediated knockdown approach. Transfection of an siRNA duplex corresponding to the BRI3BP open reading frame, but not to a scrambled (Sc) sequence, resulted in a marked decrease in the levels of BRI3BP mRNA and protein, as shown by RT-PCR and immunoblotting,

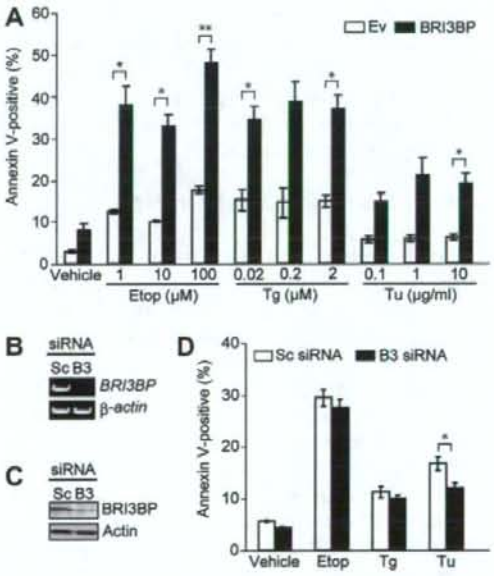

Fig. 1. Enhancement of drug-induced apoptosis by BRI3BP. (A) 293T cells transfected with either an empty vector (Ev) or the plasmid encoding the mycHis-tagged BRI3BP (BRI3BP) were pharmacologically treated for flow cytometric analysis. Annexin V positivity indicates the total percentage of two subpopulations (Annexin V^+/7-AAD^- and Annexin V^+/7-AAD^+). The result represents mean ± SEM of five separate experiments. $^*P < 0.05$, $^{**}P < 0.01$. (B,C) 293T cells were transiently transfected with siRNA duplexes for either BRI3BP (B3) or an irrelevant sequence (Sc), followed by RT-PCR and immunoblotting. (D) The siRNA-transfected cells were challenged with the vehicle, 100 μM Etop, 2 μM Tg or 10 μg/ml Tu for flow cytometry. The result represents mean ± SEM of five independent experiments. $^*P < 0.05$.

respectively (Fig. 1B and C). Tu-induced apoptosis was mitigated by BRI3BP depletion (Fig. 1D). On the other hand, apoptosis triggered by either Etop or Tg was marginally affected. Although the signaling pathways each drug utilizes for triggering apoptosis have not been elucidated in detail, death-signal cascades activated by Etop/Tg seem to be less BRI3BP-dependent than those activated by Tu. Taken together, the observed correlation between the abundance of BRI3BP and the vulnerability to pharmacological insults suggests that BRI3BP is involved in apoptosis-inducing signals emanating from the ER.

Enhanced activation of the caspase cascade by BRI3BP

We then investigated whether BRI3BP exploited the ordinary caspase signaling pathway [11] in enhancing the pharmacologically induced apoptosis of 293T cells. Because the pro-apoptotic property of BRI3BP became most clear upon treatment of the cells with Etop rather than with Tg or Tu, we analyzed the cells incubated with Etop with or without the cell-permeable pan-caspase inhibitor Z-VAD-fmk. Annexin V positivity determined by flow cytometry was decreased with Z-VAD-fmk, regardless of whether BRI3BP was transfected into the cells (Suppl. Fig. 2A). Correspondingly, the inhibitor reduced the activity of caspase-3, an effector caspase, in the Etop-treated cells as demonstrated by decreased signals derived from FITC-coupled DEVD-fmk, which irreversibly binds to activated caspase-3 (Suppl. Fig. 2B). The overexpression of BRI3BP, therefore, increases the sensitivity to Etop by upregulating the caspase cascade.

Mitochondrial damage induced by BRI3BP

The caspase-dependent facilitation of Etop-induced apoptosis by BRI3BP prompted us to examine which level along the caspase signaling pathway was modulated. The liberation of cytochrome *c* from the mitochondrial intermembrane space initiates apoptosome formation and culminates in the activation of effector caspases including caspase-3 [12,13]. Because chemotherapeutic agents trigger the mitochondrial release of cytochrome *c*, we hypothesized that this might be the step BRI3BP promoted in rendering the cells highly sensitive to Etop. The quantitation of mitochondrial cytochrome *c* content by flow cytometry revealed that BRI3BP overexpression induced an increase in the percentage of cytochrome *c*-negative subsets upon Etop treatment, indicating enhanced cytochrome *c* release (Fig. 2A). We further assessed the mitochondrial transmembrane potential ($\Delta\Psi_m$) using the membrane-permeable lipophilic cationic fluorochrome rhodamine 123 (Rh123) as a probe [9]. In response to Etop, BRI3BP-transfected cells showed $\Delta\Psi_m$ dissipation to a greater degree than mock-transfected control cells (Fig. 2B). Deterioration in mitochondrial functions, represented by both cytochrome *c* release and $\Delta\Psi_m$ collapse, is known to be closely associated with an imbalance between pro- and anti-apoptotic Bcl-2

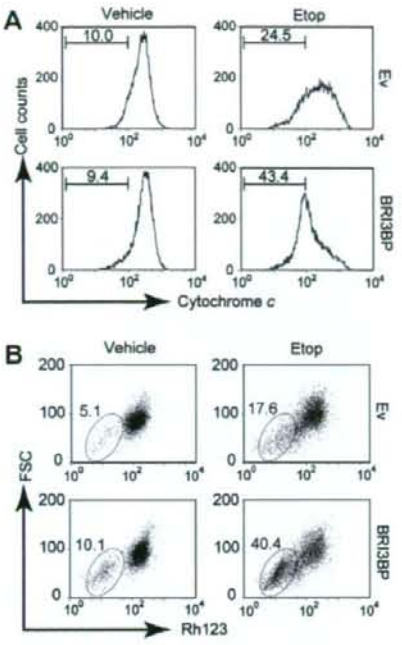

Fig. 2. Impairment of mitochondrial membrane integrity by BRI3BP overexpression. Transfected 293T cells challenged with 100 μM Etop were subjected to flow cytometric analysis of mitochondrial cytochrome *c* content (A) and transmembrane potential (B). FSC, forward light scatter. Experiments were repeated three times with similar results.

family members [14–16]. Immunoblot analysis detected no significant alterations in the expression levels of major Bcl-2 family proteins in BRI3BP-transfected cells (Suppl. Fig. 3), indicating that BRI3BP does not tip the balance, at least quantitatively, among the family members. Collectively, mitochondrial dysfunction underlies the priming of 293T cells by BRI3BP for Etop-induced apoptosis.

Absence of Etop-induced ER reorganization upon BRI3BP overexpression

Mitochondria lie adjacent to and operate in concert with the ER [17–19]. We then explored by electron microscopy the possibility that the mitochondrial dysfunction observed was secondary to the defects in the ER, where BRI3BP is localized. Treatment with the vehicle alone did not lead to a clear difference in ER morphology between mock- and BRI3BP-transfected 293T cells (Fig. 3A, B, E, and G). Upon exposure to Etop, the ER in the mock-transfected cells underwent morphological changes. It appeared in sections as whorls or a convoluted lamellar structure continuous with the nuclear membrane, to which mitochondria was frequently apposed (Fig. 3F). In contrast, such ER restructuring induced by Etop was effectively suppressed in the BRI3BP-overexpressing cells and the ER extending directly from the nuclear membrane was barely observed

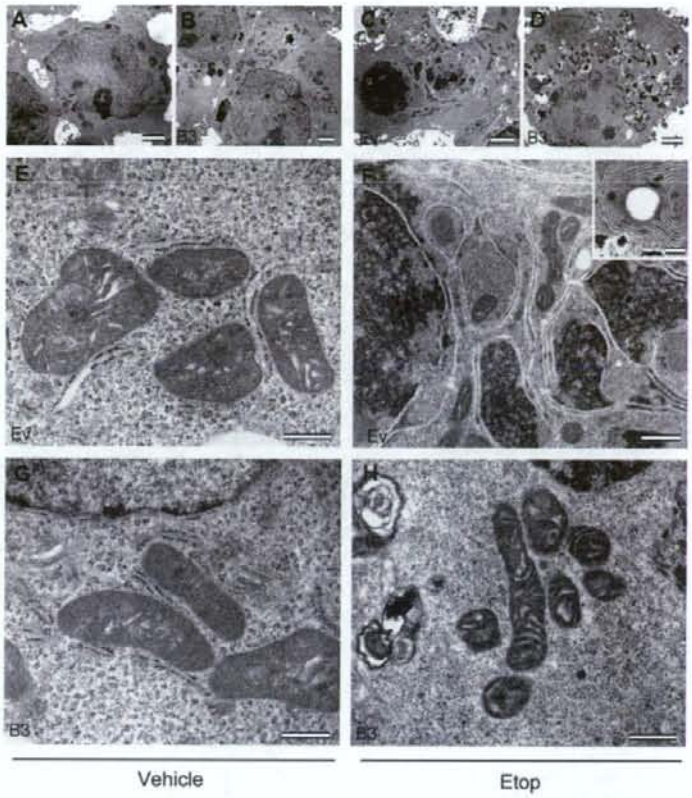

Fig. 3. Lack of ER transformation in BRI3BP-transfected 293T cells. The mock (Ev)- and the BRI3BP (B3)-transfected cells were treated with the vehicle (A, B, E, G) or 100 μM Etop (C, D, F, H) for electron microscopy. Bars, 2 μm (A–D); 0.5 μm (E–H). Data shown represent three separate experiments.

(Fig. 3H). In addition, structurally damaged mitochondria were more readily detected upon BRI3BP overexpression (Fig. 3C and D). These data suggest that the enforced expression of BRI3BP downregulates the structural plasticity of the ER, which is potentially linked to mitochondrial viability.

Discussion

In this report, we found that the BRI3BP transfection facilitates drug-induced apoptosis. It has been known that the overproduction of integral membrane proteins triggers the ER-overload response [20]. It is thus possible that the potentiation of pharmacologically induced apoptosis upon BRI3BP overexpression is attributable primarily to the excessive ER stress, but not to the specific action inherent to BRI3BP itself. However, this possibility is not supported by our data that GRP78, a chaperon induced by ER stress, was below the detection limit in both mock- and BRI3BP-transfected cells treated with either the vehicle or Etop (Suppl. Fig. 4). Therefore, in addition to BRI3BP overexpression, cofactors are required for facilitating apoptosis. This view is further supported by the fact that BRI3BP transfection alone did not induce mitochondrial dysfunction (Fig. 2).

The ER elements have various morphological forms [21,22]. It is an attractive hypothesis that the structural shift of the ER could represent a cellular adaptive response that serves to minimize the propagation of cell death signals from the ER. Because the BRI3BP overexpression inhibited Etop-induced ER restructuring (Fig. 3), it can be assumed that the facilitation of Etop-triggered apoptosis is due to the impaired plasticity of ER morphology. Major protein components of the nuclear membrane undergo caspase-dependent proteolysis in Etop-challenged cells [23]. It is therefore hypothesized that the physiological functions of the nuclear membrane are severely perturbed in BRI3BP-overexpressing cells, which showed the enhanced caspase-3 activity in response to Etop. As a result, the ER, which is structurally continuous with the nuclear membrane, might be unable to reorganize in this setting.

In this report, the relationship between the BRI3BP level and cell survival/death was analyzed *in vitro* using a cell line challenged with apoptosis inducers. If this relationship holds true *in vivo*, a reduction or loss of BRI3BP might result in the inefficient elimination of harmful cells, favoring tumor development. The array-based analysis

has demonstrated that BRI3BP mRNA levels are lower in human tumor samples (Suppl. Fig. 5), suggesting the involvement of BRI3BP in cell fate decision under physiological conditions. It is therefore possible that the BRI3BP expression level is associated with pathogenesis and that BRI3BP is a potential target of pharmacological intervention.

Acknowledgments

We are grateful to Prof. Kazuo Sugamura for continuous encouragement. This work was supported in part by grants from the Ministry of Education, Culture, Sports, Science, and Technology of Japan, the Naito Foundation, the Sumitomo Foundation, the Life Science Foundation, the Takeda Science Foundation, the Uehara Memorial Foundation, and the 21st Century Center of Excellence program.

Appendix A. Supplementary data

Supplementary data associated with this article can be found, in the online version, at doi:10.1016/j.bbrc.2007.08.082.

References

[1] R.J. Kaufman, Stress signaling from the lumen of the endoplasmic reticulum: coordination of gene transcriptional and translational controls, Genes Dev. 13 (1999) 1211–1233.
[2] D. Ron, P. Walter, Signal integration in the endoplasmic reticulum unfolded protein response, Nat. Rev. Mol. Cell Biol. 8 (2007) 519–529.
[3] C. Xu, B. Bailly-Maitre, J.C. Reed, Endoplasmic reticulum stress: cell life and death decisions, J. Clin. Invest. 115 (2005) 2656–2664.
[4] L. Lin, Y. Wu, C. Li, S. Zhao, Cloning, tissue expression pattern, and chromosome location of a novel human gene BRI3BP, Biochem. Genet. 39 (2001) 369–377.
[5] T. Katahira, Y. Imamura, D. Kitamura, The BASH/BLNK/SLP-65-associated protein BNAS1 regulates antigen-receptor signal transmission in B cells, Int. Immunol. 18 (2006) 545–553.
[6] M. Zhang, T. Yamazaki, M. Yazawa, S. Treves, M. Nishi, M. Murai, E. Shibata, F. Zorzato, H. Takeshima, Calumin, a novel Ca^{2+}-binding transmembrane protein on the endoplasmic reticulum, Cell Calcium 42 (2007) 83–90.
[7] N.J. Waterhouse, J.A. Trapani, A new quantitative assay for cytochrome *c* release in apoptotic cells, Cell Death Differ. 10 (2003) 853–855.
[8] H. Takeshima, S. Komazaki, K. Hirose, M. Nishi, T. Noda, M. Iino, Embryonic lethality and abnormal cardiac myocytes in mice lacking ryanodine receptor type 2, EMBO J. 17 (1998) 3309–3316.
[9] E. Bedner, X. Li, W. Gorczyca, M.R. Melamed, Z. Darzynkiewicz, Analysis of apoptosis by laser scanning cytometry, Cytometry 35 (1999) 181–195.
[10] I. Vermes, C. Haanen, C. Reutelingsperger, Flow cytometry of apoptotic cell death, J. Immunol. Methods 243 (2000) 167–190.
[11] I.N. Lavrik, A. Golks, P.H. Krammer, Caspases: pharmacological manipulation of cell death, J. Clin. Invest. 115 (2005) 2665–2672.
[12] D.R. Green, G. Kroemer, The pathophysiology of mitochondrial cell death, Science 305 (2004) 626–629.
[13] G. Kroemer, L. Galluzzi, C. Brenner, Mitochondrial membrane permeabilization in cell death, Physiol. Rev. 87 (2007) 99–163.
[14] J.M. Adams, Ways of dying: multiple pathways to apoptosis, Genes Dev. 17 (2003) 2481–2495.
[15] J.C. Reed, Proapoptotic multidomain Bcl-2/Bax-family proteins: mechanisms, physiological roles, and therapeutic opportunities, Cell Death Differ. 13 (2006) 1378–1386.
[16] M.F. van Delft, D.C.S. Huang, How the Bcl-2 family of proteins interact to regulate apoptosis, Cell Res. 16 (2006) 203–213.
[17] R. Rizzuto, P. Pinton, W. Carrington, F.S. Fay, K.E. Fogarty, L.M. Lifshitz, R.A. Tuft, T. Pozzan, Close contacts with the endoplasmic reticulum as determinants of mitochondrial Ca^{2+} responses, Science 280 (1998) 1763–1766.
[18] L. Scorrano, S.A. Oakes, J.T. Opferman, E.H. Cheng, M.D. Sorcinelli, T. Pozzan, S.J. Korsmeyer, BAX and BAK regulation of endoplasmic reticulum Ca^{2+}: a control point for apoptosis, Science 300 (2003) 135–139.
[19] G. Csordas, C. Renken, P. Varnai, L. Walter, D. Weaver, K.F. Buttle, T. Balla, C.A. Mannella, G. Hajnoczky, Structural and functional features and significance of the physical linkage between ER and mitochondria, J. Cell Biol. 174 (2006) 915–921.
[20] H.L. Pahl, P.A. Baeuerle, The ER-overload response: activation of NF-κB, Trends Biochem. Sci. 22 (1997) 63–67.
[21] C.M. Federovitch, D. Ron, R.Y. Hampton, The dynamic ER: experimental approaches and current questions, Curr. Opin. Cell Biol. 17 (2005) 409–414.
[22] N. Borgese, M. Francolini, E. Snapp, Endoplasmic reticulum architecture: structures in flux, Curr. Opin. Cell Biol. 18 (2006) 358–364.
[23] B. Buendia, A. Santa-Maria, J.C. Courvalin, Caspase-dependent proteolysis of integral and peripheral proteins of nuclear membranes and nuclear pore complex proteins during apoptosis, J. Cell Sci. 112 (1999) 1743–1753.

第４回（平成１８年度）薬学研究ビジョン部会部会賞受賞者（１）

ケミカル・バイオ情報に基づく創薬インフォマティクス研究

奥野　恭史　京都大学大学院薬学研究科　統合薬学フロンティア教育センター

１、はじめに

ヒトゲノムが解読された今日、莫大なゲノム情報から創薬への手がかりを発見すること、すなわち「ゲノム創薬」に大きな期待が寄せられている。ゲノム創薬は、ゲノム情報を出発点とし創薬の標的遺伝子探索からリード化合物探索を経て臨床段階に至る広範で高度に専門化した複合領域であり、その実践にはこれらの複合領域の橋渡しを実現する統合的なインフォマティクス基盤（創薬インフォマティクス）が必須となる。我々は、創薬インフォマティクスという新たな研究分野の創成に向け、バイオ情報を扱うバイオインフォマティクスとケミカル情報を扱うケモインフォマティクスの独立に発展してきた２つの情報科学分野の統合を図り、バイオ情報とケミカル情報の両者を同時に統合的にマイニングする新しい情報技術の開発に着手している。さらに本研究は、現在、国内外で注目されているケミカルゲノミクス・ケミカルバイオロジーのための有力な情報基盤ともなり得るものと考えられる。

２、化合物の宇宙探索（ケミカル空間の探索）

2004 年 12 月の Nature 誌において、Chemical Space 特集号が発表された(1)。そこでは、化合物の種類は 1060 個を越える天文学的なバリエーションを有しており、化合物空間を探索することは宇宙探索と同様に壮大な課題であることが提示されている。このことは医薬品の候補化合物となり得る新規な活性化合物を見つけ出すことが如何に困難でセレンディップなことであるかを示唆するものである。

これらケミカル空間の探索の基礎研究としてケミカルゲノミクス・ケミカルバイオロジー研究が近年注目されている。ケミカルゲノミクスでは、その命題として「莫大な数の化合物と生体系（タンパク質や細胞など）との相互作用を包括的に明らかにすること」が挙げられている。実際、米国では、ケミカルゲノミクスプロジェクトを掲げ、数百万もの膨大な化合物に関する情報を収集し、有用化合物の探索に国策として取り組んでいる。

しかしながら、広大な化合物空間から生物活性を有する化合物を探し当てる化合物探索には、天文学的な数量に対応できる新たなインフォマティクス技術とハイスループット技術の研究開発が必須である。そこで、我々は、莫大な化合物群とタンパク質群との相互作用様式をゲノムスケールで解析することを目的とした情報学的技術、すなわちケミカルゲノミクスのためのインフォマティクス技術の研究開発を行っている。

３、ケモインフォマティクスとバイオインフォマティクス（図１）

ケミカルゲノミクス・ケミカルバイオロジーでは、化合物のケミカル情報と生体系のバイオ情報の２種の異なる情報が対象となる。従って、ケミカルゲノミクスのための情報処理技術には、ケミカル情報を処理するケモインフォマティクスとバイオ情報を処理するバイオインフォマティクスを融合する新たなインフォマティクス技術の開発が必須となる。しかしながら、化学と生物学という異なる分野を背景にもつ２つのインフォマティクスは、独立して発展してきており現状では互いに相容れない。そこで、我々はケモインフォマティクスとバイオインフォマティクスにおける方法論的なアナロジーに着目しその融合を図った。すなわち、ケモインフォマティクスもバイオインフォマティクスも共に、個体（化合物やタンパク質）の特徴量を数値やベクトルで表現することにより、各個体の相対的な特性の違いを探索空間上の個体間の距離として定量的に算出する方法論を基本としている。例えば、ケモインフォマティクスでは、データベースに集積された膨大な化合物エントリーは化学構造や特性を定量的に表すベクトルとして表現され、その相対的な違いを距離の尺度として持つ座標空間(探索空間)をコンピュータ内部に構築する。データベース検索はこの探索空間において距離が近接する化合物を類似化合物として選出してくることに

なる。また、バイオインフォマティクスでも同様の考え方であり、遺伝子・タンパク質エントリーは配列や構造として表現され、それぞれの相同性（類似度）を尺度として持つ探索空間（バイオデータの場合、探索空間は系統樹やネットワーク構造になっている場合もある。）が構築され、データベース検索にはこの探索空間に基づき、類似（類縁）遺伝子・タンパク質が選出される。

一方、ケミカルゲノミクスとは、ケミカル空間の個体（化合物）とバイオ空間の個体（遺伝子・タンパク質）との相互作用関係を網羅的に明らかにする研究であり、図1の赤線に示す対応関係を付加したモデルであると考えられる。ここで、我々は、ケミカル情報とバイオ情報を統合的に処理するために、ケミカル空間（緑色）とバイオ空間（黄色）を独立して扱うのではなく、2つの空間を融合したモデルをケミカルゲノミクスのためのインフォマティクスモデルとして初めて考案した。

図1．ケモインフォマティクスとバイオインフォマティクス

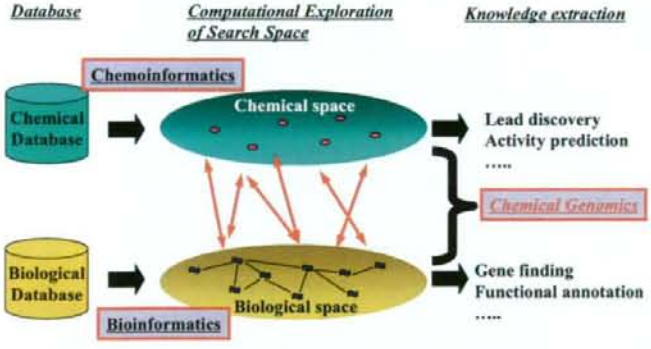

4、ケミカル空間−バイオ空間の融合モデル

情報科学的アプローチによる化合物探索は、これまで化合物のケミカル情報のみを用いたケモインフォマティクス手法が用いられてきた。これに対し、我々の手法は、このケミカル情報のみの従来手法にバイオインフォマティクス技術を融合させ、バイオ情報を考慮に入れた化合物探索を実現する新しいインフォマティクス手法と言える。（図1）

例えば、化合物について構造や特性の類似性を相対的な位置関係として表現したものをケミカル空間（赤が化合物、緑領域がケミカル空間）として定義するとともに、タンパク質についても類似関係（配列や構造の相同性）を相対的な位置関係として表現したものをバイオ空間（青がタンパク質、黄色領域がバイオ空間）として定義する。さらに個々の化合物とタンパク質の結合をリンク（黒線）することによって、これらケミカル空間とバイオ空間を融合した単純モデルをコンピュータ内部に構築できる。（図2）

ここで、標的タンパク質に作用する化合物候補を探索するIn silicoスクリーニングにこの融合モデルを適用する場合を考えると、

1）標的タンパク質（青星）の配列構造から、そのタンパク質がバイオ空間座標にマッピングされる。

2）バイオ空間にマッピングされた標的タンパク質の近隣タンパク質からのケミカル空間へのリンク情報をたどること（青矢印）により、その標的タンパク質が関係するケミカル空間のエリア（青円内）を指定することができる。

3）上記エリア内の化合物群が、標的タンパク質に相互作用する可能性のある化合物群と推定される。（ここでは、類似のタンパク質は、類似の化合物を結合するという前提を基にしている。）

図2．ケミカル空間−バイオ空間融合モデルを用いたIn silicoスクリーニング

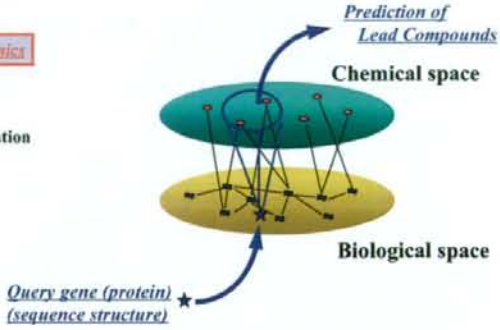

我々は、このケミカル空間とバイオ空間の融合モデルを用いた探索を、GPCRファミリーとそのリガンド化合物の探索に適用し、GLIDAデータベース(2,3)としてWebサービスを行っている。

5、ケミカル空間−バイオ空間の相関モデル

我々が考案する融合モデルで最も重要なことは、モデルの構築方法である。我々の方法は、こ

のモデル構築方法においても、従来法より大きな優位性を有している。

ケミカル空間の構築に用いられる従来法の代表的なものに主成分分析(PCA)がある。これは、ケミカル情報のみを用い、化合物の化学特性ができる限り多様になるように、ケミカル空間座標を定義するものであり、ここでの大きな問題点は、化合物の多様性と生物活性との直接の因果関係は無いということである。

これらの問題点を克服することを目的とし、我々は正準相関分析（CCA）を用いて相関モデル構築を試みた。本手法は、ケミカル情報とタンパク配列情報の両情報を用いて、ケミカル空間とタンパク空間の両空間の相関が高くなるように互いの空間座標を定義するものである。これはバイオ空間の分布を考慮して、ケミカル空間座標を定義する方が、生物活性にとって都合の良い空間座標を構築できるという大きな特徴を有する。

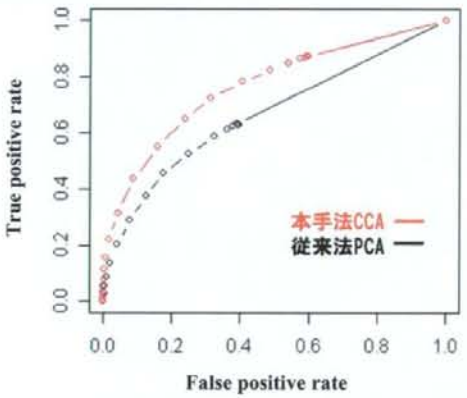

図３．本手法と従来法との性能比較

実際に、従来法(PCA)と本手法(CCA)の性能を比較するために、既知データ(DrugBank データベース(4))を用いた 5-fold cross validation テストを実施し、化合物とタンパク質の相互作用予測の予測性能評価を行った。その結果を図 3 に示す。図は、予測性能を評価する有名な方法の一つである ROC 曲線（横軸は化合物-タンパク質相互作用を誤って予測した割合、縦軸は正しく予測した割合を示す。）であり、このグラフは曲線が上に位置するほど、予測性能が良いことを表す。本手法の赤曲線が従来法の黒曲線より上方に位置することから、本手法の方が、従来法よりも高い予測性能であることがわかる。

6、Biologically relevant chemical space

ごく最近、宇宙観測において、暗黒物質（ダークマター：目には見えない物質）の宇宙空間での分布が初めて観測され宇宙の起源解明に期待が寄せられている。化合物の宇宙空間では、我々は何を探索しなければならないのであろうか？Chemical Space 特集号では、その答えとして「生物にとって意味のある化合物群（Biologically relevant chemical space)」を探索することの重要性を提示している。しかしながら、Biologically relevant chemical space を定義する具体的方法に関する報告は未だなされていない。

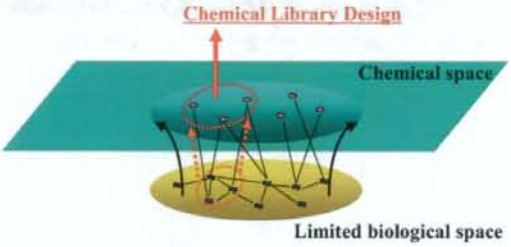

図４．Biologically relevant chemical space

我々の開発した融合モデルはこの難問に一つの解答を与える事ができ、タンパク質群と化合物群の相互作用様式の統計モデルを構築することにより、広大なケミカル空間のうち黄色のバイオ空間に対応するケミカル空間（biologically relevant chemical space）を限定することを可能にする。(図 4) また、バイオ空間のタンパク群を、例えば GPCR ファミリー（赤点線エリア）などに限定することにより GPCR 用のフォーカスライブラリーの設計も可能になり、生物活性を有する化合物ライブラリーの合理的設計が実現できる。

例えば、図 5 は、カナダでサービスされている DrugBank データベース(4)における 3476 個の既知薬物ターゲットタンパク質からなるバイオ空間とそれに対応する 3079 個の既知薬物からなるケミカル空間の実際の相関モデルである。このように、Biologically relevant chemical space の定義が可能となる。